Laser and Particle Beams (2017), *35*, 42–47.

doi:10.1017/S0263034616000781

Low-temperature photoionized plasmas induced in Xe gas using an EUV source driven by nanosecond laser pulses

A. BARTNIK, W. SKRZECZANOWSKI, P. WACHULAK, I. SABER, H. FIEDOROWICZ, T. FOK, AND Ł. WĘGRZYŃSKI

Institute of Optoelectronics, Military University of Technology, Kaliskiego 2, 00-908 Warsaw, Poland

(Received 12 October 2016; Accepted 12 November 2016)

Abstract

In this work, a laser-produced plasma source was used to create xenon (Xe) photoionized plasmas. An extreme ultraviolet (EUV) radiation beam was focused onto a gas stream, injected into a vacuum chamber synchronously with the EUV pulse. Energies of photons exceeding 100 eV allowed for inner-shell ionization of Xe atoms. Creation of *N*-shell vacancies resulted in *N*-shell fluorescence and was followed by multiple ionization. Time-integrated EUV spectra, corresponding to excited states in Xe II–V ions, were recorded. Several emission lines detected in the 39–65 nm wavelength range were not reported earlier. They were not identified due to lack of a corresponding information in published databases. Except spectral measurements in the EUV range, time resolved ultraviolet and visible spectra, originating from Xe II and III ions, were recorded. For spectral lines, corresponding to radiative transitions in Xe II ions, electron temperature was calculated based on a Boltzmann plot method. Based on this method the temperature was measured for different time delays according to the driving EUV pulses.

Keywords: Laser plasma; Extreme ultraviolet; Photoionization

1. INTRODUCTION

Low-temperature plasmas used in technology can be produced using various plasma generators, including inductively or capacitively coupled radiofrequency plasma reactors (Peignon *et al*., 1991; Plank *et al*., 2003; Lallement *et al*., 2010; Shim *et al*., 2012), microwave plasma torch (Hong *et al*., 2006), dielectric barrier discharge (Korotkov *et al*., 2007), or electron-beam-generated plasmas (Baraket *et al*., 2010). All these generators can produce different kinds of low-temperature plasmas, including reactive plasmas. The electron temperature in case of IC–RF plasmas is at the level of 1–8 eV. In case of the electron-beam-generated plasmas or atmospheric plasmas, the temperature is lower, within the range of 0.4–0.6 eV. Their electron density is of the order of 10^{11} cm^{-3}; however, in case of atmospheric plasmas it can reach the value of 10^{13} cm^{-3} (Ogura *et al*., 1997). Plasmas produced in this way are used in industrial processes, such as gas phase plasma chemistry, surface treatment, and coating. Treatment of some materials, employing reactive low-temperature plasmas, results in formation of volatile products such as FW_6 (Peignon *et al*., 1991), GeF_4 (Peignon *et al*., 1991), or SiF_4 (Liptak *et al*., 2009). This effect can be thus utilized for reactive plasma etching of tungsten, germanium, silicon, or other materials containing these elements such as SiC (Plank *et al*., 2003) or glass (Lallement *et al*., 2010). Such etching processes are employed in microelectronic technologies for the fabrication of semiconductor devices, microengineering, nanotechnology, etc.

Low-temperature plasmas are also present in the Space. They can be encountered in planetary or star atmospheres, for example. In the first case, upper planetary atmospheres are ionized by solar radiation, composed of either high-energy photons or charged particles. In case of molecules, interaction with high-energy photons results in their dissociation to ionic or neutral species. Ionization of O_2, N_2, and other simple molecules by solar radiation is one of the most important ion production channels on Earth's and Titan's (Huebner *et al*., 1992; Dutuit *et al*., 2013; Pavlov, 2014) upper atmospheres. Photoionization of atoms and molecules is one of the dominant processes forming the thermosphere (Peterson *et al*., 2012, 2013). Different kinds of molecular processes that can be encountered in such conditions are simulated in laboratory employing synchrotrons (Imanaka & Smith, 2009; Pilling *et al*., 2011) or plasma discharge sources (Kołos, 1995).

Address correspondence and reprint requests to: A. Bartnik, Institute of Optoelectronics, Military University of Technology, Kaliskiego 2, 00-908 Warsaw, Poland. E-mail: andrzej.bartnik@wat.edu.pl

Laboratory simulations are devoted also to low-temperature plasmas present in atmospheres of stars. Some experiments concern, for example, white dwarf (WD) photospheres (Falcon *et al*., 2010, 2013). To perform the experiments a special gas cell was mounted close to the high-temperature, high-density *z*-pinch plasma produced at *Z*-pulsed power facility (Matzen *et al*., 2005). In this case, photoionized hydrogen plasma with a temperature of approximately 1 eV and an electron density of 10^{17} cm^{-3} can be created. These parameters are similar to the parameters of the WD photospheres allowing us to perform some benchmark measurements concerning calibration of WD atmosphere models.

In this work, spectral investigations of low-temperature xenon (Xe) photoionized plasmas, induced using a laser-produced plasma (LPP) extreme ultraviolet (EUV) source, were performed. The source is based on a nanosecond Nd:YAG laser and a double-stream gas puff target. The radiation was focused employing a reflective EUV collector. Low-temperature Xe plasmas, composed of multiply charged ions, were produced. Plasmas were investigated by time-integrated spectral measurements in the EUV range and time-resolved spectroscopy in the ultraviolet and visible (UV/VIS) range. Several unidentified lines in the EUV spectral range were detected. Based on the spectral measurements a temporal evolution of relative intensities of selected spectral lines and the electron temperature was determined. Origin of doubly and triply charged ions was discussed.

2. EXPERIMENT

The experimental setup consisted of a LPP EUV source, an injection system for delivering of small portions of Xe gas into an interaction region, synchronized with the EUV source, and the spectral measurement system. The LPP EUV source was based on a 0.8 J/4 ns/10 Hz Nd:YAG laser, manufactured by EXPLA Company and a double stream gas puff target, described elsewhere (Fiedorowicz *et al*., 2000; Bartnik *et al*., 2001). The laser plasma was created in a Xe stream allowing for strong emission of radiation in the EUV range. Thousands of overlapping spectral lines formed a quasi-continuous spectrum with the most intense emission at the wavelength range $\lambda \approx 11 \pm 1$ nm. Part of the EUV radiation emitted from the Xe plasma into the 4π sr sphere was focused using an axi-symmetrical grazing incidence ellipsoidal collector (Rigaku Innovative Technologies Europe s.r.o., Czech Republic). Diameter of the focal spot (full width at half maximum (FWHM) of the intensity distribution) was approximately 1.5 mm and a maximum EUV fluence reached 0.1 J/cm^2. The Xe gas was injected into the vacuum chamber, synchronously with the EUV pulses, using an auxiliary gas puff valve. The valve, equipped with a cylindrical nozzle, was mounted such as, to assure injection of the gas perpendicularly to an optical axis of the EUV collector. The gas density in the interaction region was controlled by an opening time of the valve or adjustment of a backing pressure. The gas density adjusted this way was of the order of 1/10% of the atmospheric density. Interaction of the EUV beam with the Xe gas resulted in creation of the low temperature, photoionized plasma, emitting radiation in an optical and EUV range.

The measurement system consisted of two spectrographs. The first one was an EUV spectrograph (McPherson, Model 251) allowing for time-integrated measurements. The spectrograph was equipped with a grazing incidence, flat-field toroidal grating having a groove density 450 g/mm. Its spectral range was $\lambda \approx 10$–95 nm and the resolution for the wavelength of $\lambda = 50$ nm was approximately $\lambda/\Delta\lambda \approx 500$. The spectra were acquired using a back-illuminated CCD detector (Princeton Instruments Inc.). To minimize a thermal noise the detector was cooled down to a temperature of −65 °C. The second spectrograph was an Echelle Spectra Analyzer ESA 4000, equipped with the ICCD Kodak KAF 1001 camera, allowing for time-resolved measurements. Its spectral range covered the UV/VIS wavelengths, $\lambda = 200/780$ nm. The spectral resolution was approximately $\lambda/\Delta\lambda \approx 20{,}000$. Optical axes of both spectrographs were orthogonal with respect to the optical axis of the EUV irradiation system. For such configuration, weak spectra originating from photoionized plasmas were not affected by the strong laser plasma radiation. More details concerning the experimental setup can be found elsewhere (Bartnik *et al*., 2011, 2012).

3. EXPERIMENTAL RESULTS

The time-integrated emission spectra, originating from the Xe photoionized plasmas, recorded in the EUV range, were very weak. To obtain spectral intensities sufficient for further analysis, a multiple exposure spanning thousands of spectral signals was necessary. Typical spectra presented in Figures 1 and 2 were obtained by accumulation of 4000 pulses. The emission spectrum, shown in Figure 1 contains two pronounced fluorescent lines corresponding to inner shell $5s^24d^{10}5p^5$–$5s^24d^95p^6$ transitions, $^2D_{5/2}$–$^2P_{1/2}$ (λ =

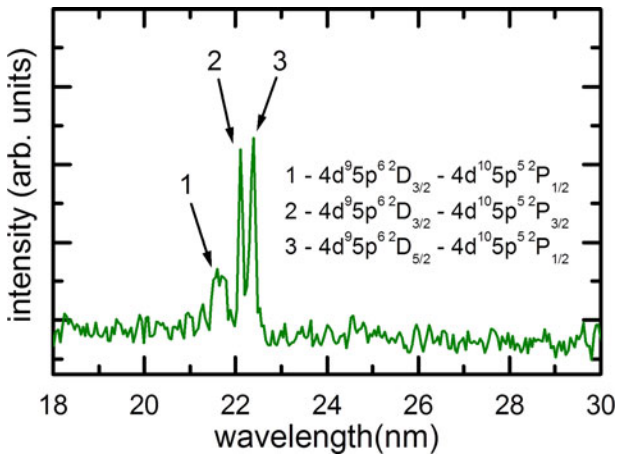

Fig. 1. *N*-shell spectrum of Xe II ions.

https://doi.org/10.1017/S0263034616000781 Published online by Cambridge University Press

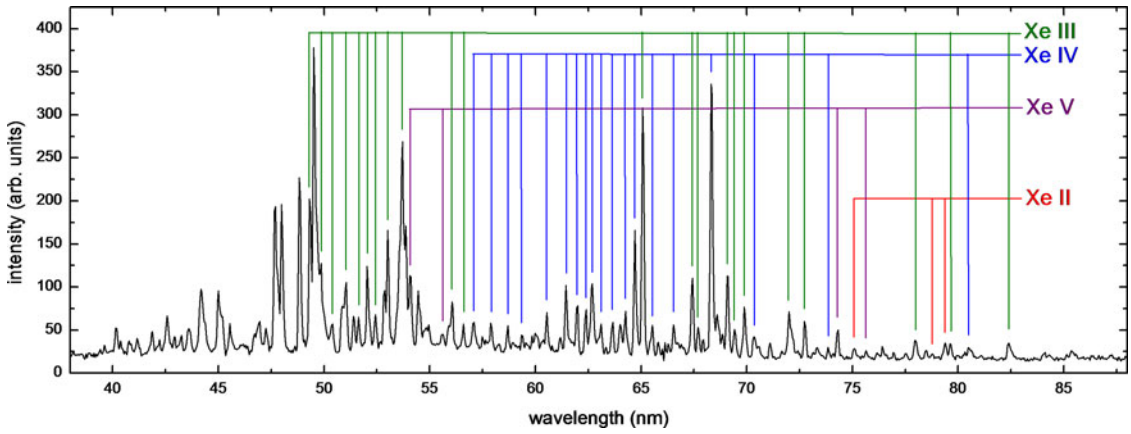

Fig. 2. EUV spectrum of Xe ions.

22.39 ± 0.05 nm) and $^2D_{3/2}$–$^2P_{3/2}$ (λ = 22.11 ± 0.05 nm), following the *N*-shell photoionization. The additional broad peak of significantly lower intensity at the wavelength of λ = 21.6 nm can be attributed to the $^2D_{3/2}$–$^2P_{1/2}$ transition.

The second part of the EUV spectrum, spanning the wavelength range of 40–85 nm, is shown in Figure 2. It consists of multiple lines, originating mainly from transitions in singly to quadruply charged ions. The spectral lines correspond mainly to $5s^25p^k$–$5s^25p^{k-1}5d$, $5s^25p^k$–$5s^25p^{k-1}6s$, $5s^25p^k$–$5s^25p^{k-1}6d$ and $5s^25p^k$–$5s5p^{k+1}$ transitions, where k = 5–2 for Xe II–V, respectively. All the lines were identified based on the NIST (http://physics.nist.gov/PhysRefData/ASD/lines_form.html) database and the references contained therein. There were also several lines detected, especially in the wavelength range of 40–49 nm, not found in any database. Wavelengths of these lines, together with their relative intensities, are presented in Table 1. The relative intensities were referred to the line intensity of Xe III ions at the wavelength of λ = 65.048 nm, with the relative intensity equal to 12, according to the NIST data.

Besides the EUV spectra also the UV/VIS spectra were recorded. These spectra could be acquired with temporal resolution. The narrowest possible gate time was 20 ns. In our experiments, the 40 ns gate time was employed. A typical spectrum acquired at the early stage of photoionized plasma formation is presented in Figure 3.

The spectrum consists of multiple lines corresponding to radiative transitions in singly and doubly charged ions. Most of the lines and the most intense ones originate from transitions in Xe II ions. For two of these lines with the wavelengths of λ_1 = 484.433 and λ_2 = 229.652 nm, respectively, temporal evolution is presented in Figure 4. As could be expected their intensities are monotonically decreasing with the delay time between the moment of formation of the photoionized plasma and the spectral acquisition; however, the decrease is not very fast, several times longer comparing to the time duration of the driving pulse. Similar decrease concerns most of the other lines detected in the UV/VIS spectral region.

4. DISCUSSION OF THE RESULTS

The EUV photons, used for creation of photoionized plasmas in this work, have energies up to approximately 140 eV with the maximum of spectral intensity at about 110 eV. In case of neutral Xe, the energies of photons, required for creation of the inner shell $Xe^+4d^9\ ^2D_{3/2}$ and $Xe^+4d^9\ ^2D_{5/2}$ states, have to exceed the corresponding binding energies, which are 69.29 and 67.32 eV, respectively (Fritzsche *et al.*, 2011). Thus, these states can be easily created producing a large number of photoelectrons. Creation of the inner shell

Table 1. *Wavelengths and relative intensities of spectral lines in the EUV range not published in the NIST or other databases for the low-charged Xe ions.*

Sl. no.	Wavelength (nm) λ ± 0.05 nm	Relative intensity (arb. units)
1	39.61	0.4
2	40.19	1.1
3	40.38	0.6
4	40.77	0.6
5	41.16	0.7
6	41.89	1
7	42.23	0.6
8	42.57	1.7
9	42.91	0.7
10	43.25	0.8
11	43.59	1.1
12	44.17	2.9
13	45.00	2.8
14	45.54	1.3
15	46.96	1.4
16	47.26	1.1
17	47.7	6.6
18	47.99	6.7
19	48.85	8
20	49.51	13.8
21	51.41	1.7
22	52.87	2.8
23	54.46	2.8
24	64.02	1.3

https://doi.org/10.1017/S0263034616000781 Published online by Cambridge University Press

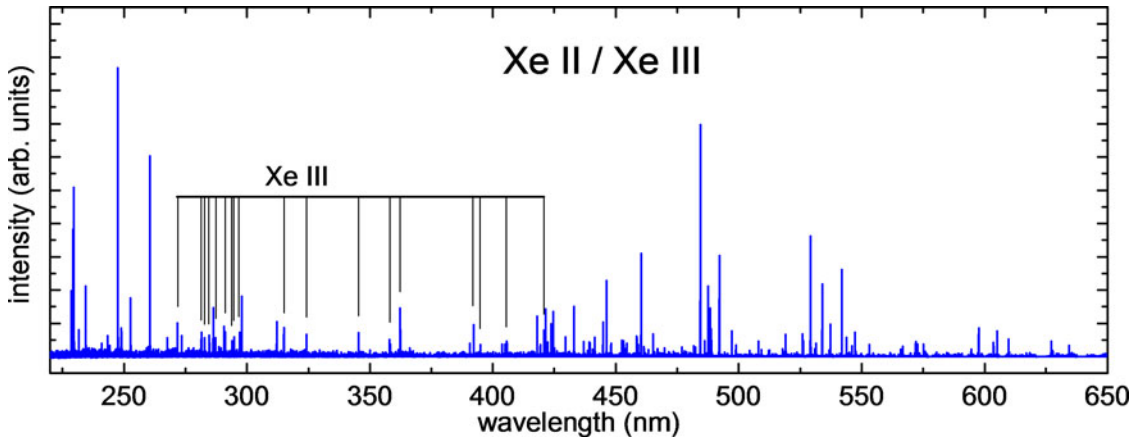

Fig. 3. UV/VIS spectrum of Xe ions.

vacancies is followed by EUV fluorescence with the spectrum presented in Figure 1 or the Auger decay to doubly or triply charged ions. It should be pointed out that the fluorescence probability for the $Xe^{+}4d^{9}$ states is a few orders of magnitude smaller comparing with the Auger decay. It means that practically all of these states relax producing Auger electrons that, similarly to photoelectrons, have energies sufficient for further ionization of Xe atoms or single-charged ions. Ionization thresholds of Xe III and IV ions, produced due to a single or double Auger decay are 31.05 and 40.9 eV, respectively (Saloman, 2004). It can be easily calculated that energies of the photo- and Auger electrons are sufficient for further ionization or excitation of these ions, as well. A radiative decay of the excited states of Xe III and IV ions results in the EUV spectrum shown in Figure 2. It can be noticed that the most intense lines originate from these ions. Some of the lines with relatively low intensities can be attributed to the excited Xe atoms or Xe II and Xe ions. There are also a number of spectral lines detected in the EUV range, enumerated in Table 1. These lines were not reported in the NIST or other published databases for the low-charged Xe ions. It suggests that these lines are not encountered in typical, low-temperature plasmas, employed for spectral investigations, and are specific for the photoionized Xe plasma produced in the experiment described in this work. Their emission can be associated with the photoionization/photoexcitation processes and ionization or excitation by non-thermal electrons, producing inner-shell vacancies or multi-excited states.

Thermalization of photo- and Auger electrons leads to formation of low-temperature plasmas. The electron temperature and its temporal evolution were estimated based on a Boltzmann plot method (Harilal, 2004; Aragón & Aguilera, 2008). The corresponding plots were constructed for emission spectra recorded in the UV/VIS range. An example of such spectrum is presented in Figure 3. The Boltzmann plot constructed for this spectrum, shown in Figure 5, was based on Xe II lines. The plot employs relative intensities I_{ki} of spectral lines, corresponding to radiative transitions between the levels i and k. The individual points correspond to the values of $\ln(I_{ki}\lambda_{ki}/A_{ki}g_k)$ versus the upper-level energy E_k. In this case, λ_{ki} is the wavelength, A_{ki} the radiative transition probability and g_k is the statistical weight of the upper

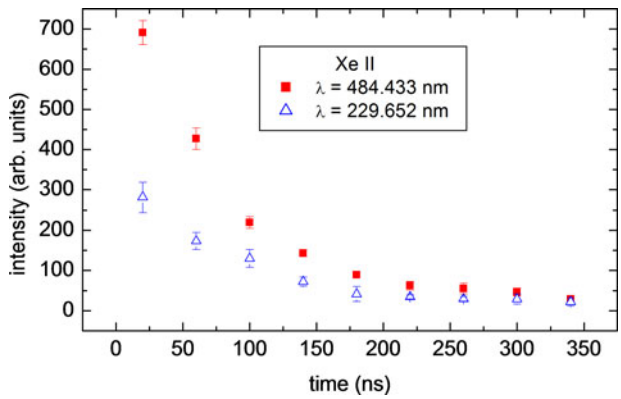

Fig. 4. Temporal evolution of two Xe II spectral lines.

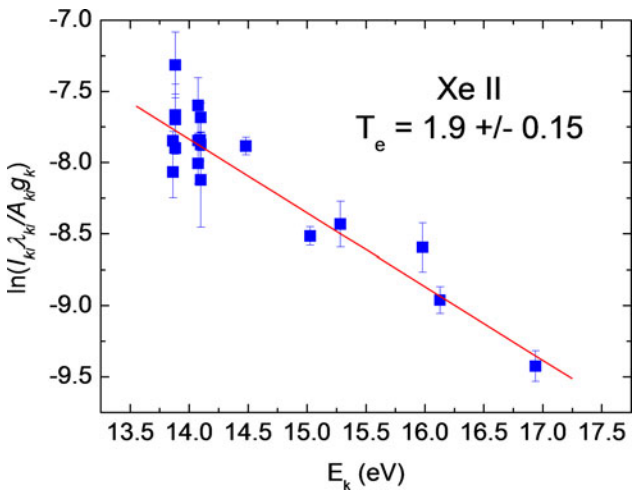

Fig. 5. An example of the Boltzmann plot constructed for Xe II emission lines recorded in the UV/VIS range.

https://doi.org/10.1017/S0263034616000781 Published online by Cambridge University Press

level. In case of plasmas being in a local thermodynamic equilibrium (LTE) or at least pLTE (partial LTE) a straight line can be fitted to the points and the slope $1/kT$ yields the electron temperature. All the data points used for the determination of the electron temperature correspond to individual lines not overlapping with other lines. To estimate the measurement uncertainty, five spectra were taken into account for construction of a particular Boltzmann plot. The uncertainty is connected with shot-to-shot variation of the photoionized plasma parameters and some deviation from the LTE conditions. The variation of plasma parameters can be attributed to small differences between energies and spectral profiles of the driving EUV pulses, at the level of 5–10%. These differences originated mainly from variation of parameters of the gas puff target used for the laser plasma creation. A similar variation concerned the density of the Xe gas injected into the interaction region for creation of photoionized plasmas. As a result, the emission spectra obtained from successive pulses were slightly different. The line intensities were determined by numerical integration of the line profiles. The corresponding data points were calculated based on the formula $\ln(I_{ki}\lambda_{ki}/A_{ki}g_k)$ and averaged over five spectral distributions. Standard deviations from the averaged values were calculated for each point and marked in Figure 5 as error bars.

Based on analogous Boltzmann plots based on Xe II spectra recorded for different time delays in respect to the exciting EUV pulses, a time dependence of the electron temperature was determined. The corresponding graph is shown in Figure 6. It should be pointed out, that even though the temperature is decreasing, the decrease is relatively slow. The temperature is maintained at the level of 1–2 eV within the time of 300 ns.

It should be pointed out that the temperature decrease is significantly slower comparing to the decrease of spectral lines intensities shown in Figure 4. It is clear taking into account that most of the excited Xe II states are produced at the beginning in the non-LTE plasma. After that the energies of photo- and Auger electrons are continuously decreasing due to bound-free and free–free processes and their energy distribution becomes Maxwellian. Most of thermalized electrons have energy too low for ionization or excitation of Xe ions; hence, their average energy is decreasing relatively slowly.

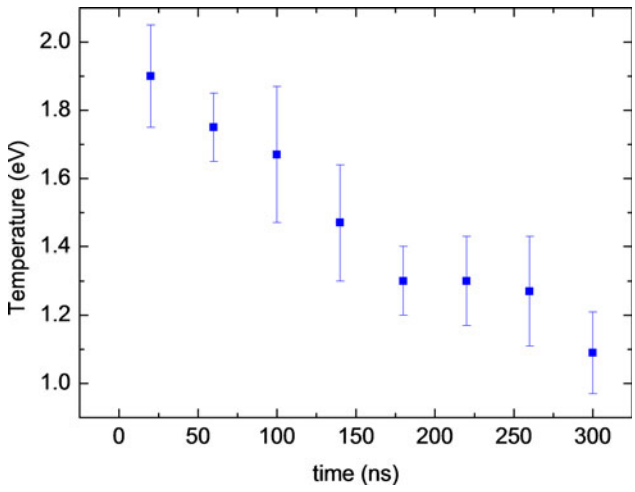

Fig. 6. Time dependence of the photoionized plasma electron temperature.

5. SUMMARY

In this work, the first results of investigations of EUV induced low-temperature photoionized Xe plasmas are presented. Plasmas were created by irradiation of small portions of Xe gas, using the 10 Hz LPP source, equipped with the ellipsoidal collector. The gas was delivered into the interaction region synchronously with the EUV pulses. The resulting low-temperature photoionized plasmas were investigated using the EUV and UV/VIS spectroscopy. Low-intensity EUV spectra consisted of emission lines corresponding to transitions in Xe II–V ions. Most of the spectral lines were identified. Several lines, however, detected in the EUV range, were not reported in known, published databases. Their presence is interpreted to be specific for the EUV-induced photoionized Xe plasmas, where inner-shell vacancies can significantly modify population of the excited states. Such conditions can be created during irradiation of Xe gas by the intense EUV pulses, when intense photoionization governs the plasma formation process.

In case of the UV/VIS spectra, only emission lines corresponding to excited states in singly and doubly charged ions were detected. It was assumed that population of these states is determined mainly by collisional processes, following the photoionization phase, and the pLTE plasma is being formed. In this case, for spectral lines corresponding to radiative transitions in Xe II ions, Boltzmann plots were constructed and temporal evolution of the electron temperature was determined. It was shown that the temperature of the order of 1 eV is maintained during a relatively long time, at least 300 ns, which is two order of magnitude longer comparing with the duration of the exciting EUV pulse.

ACKNOWLEDGMENTS

This work was supported by the National Science Centre, Poland, grant agreement no. UMO-2013/09/B/ST2/01625, and partially by European Union's Horizon 2020 Program (LASERLAB-EUROPE) grant agreement no. 654148

REFERENCES

Aragón, C. & Aguilera, J.A. (2008). Characterization of laser induced plasmas by optical emission spectroscopy: A review of experiments and methods. *Spectrochim. Acta B* **63**, 893–916.

Baraket, M., Walton, S.G., Lock, E.H., Robinson, J.T. & Perkins, F.K. (2010). The functionalization of graphene using electron-beam generated plasmas. *Appl. Phys. Lett.* **96**, 231501.

Bartnik, A., Fiedorowicz, H., Jarocki, R., Kostecki, J., Szczurek, M. & Wachulak, P.W. (2011). Laser-plasma EUV source

https://doi.org/10.1017/S0263034616000781 Published online by Cambridge University Press

dedicated for surface processing of polymers. *Nucl. Instrum. Methods Phys. Res. A* **647**, 125–131.

Bartnik, A., Fiedorowicz, H., Rakowski, R., Szczurek, M., Bijkerk, F., Bruijn, R. & Fledderus, H. (2001). Soft x-ray emission from a double stream gas puff target irradiated by a nanosecond laser pulse. *Proc. SPIE 4424 ECLIM 2000* (M. Kalal, K. Rohlena, M. Sinor, Eds), Prague, Czech Republic, pp. 406.

Bartnik, A., Lisowski, W., Sobczak, J., Wachulak, P., Budner, B., Korczyc, B. & Fiedorowicz, H. (2012). Simultaneous treatment of polymer surface by EUV radiation and ionized nitrogen. *Appl. Phys. A* **109**, 39–43.

Dutuit, O., Carrasco, N., Thissen, R., Vuitton, V., Alcaraz, C., Pernot, P., Balucani, N., Casavecchia, P., Canosa, A., Le Picard, S., Loison, J.C., Herman, Z., Zabka, J., Ascenzi, D., Tosi, P., Franceschi, P., Price, S.D. & Lavvas, P. (2013). Critical review of N, N^+, N_2^+, N^{++}, and N_2^{++} main production processes and reactions of relevance to Titan's atmosphere. *Astrophys. J. Suppl. Ser.* **204**, 20.

Falcon, R.E., Rochau, G.A., Bailey, J.E., Ellis, J.L., Carlson, A.L., Gomez, T.A., Montgomery, M.H., Winget, D.E., Chen, E.Y., Gomez, M.R. & Nash, T.J. (2013). An experimental platform for creating white dwarf photospheres in the laboratory. *High Energy Density Phys.* **9**, 82–90.

Falcon, R.E., Rochau, G.A., Bailey, J.E., Ellis, J.L., Montgomery, M.H., Winget, D.E., Gomez, M.R. & Leeper, R.J. (2010). Creating white dwarf photospheres in the laboratory. *AIP Conf. Proc.* **1273**, 436.

Fiedorowicz, H., Bartnik, A., Jarocki, R., Rakowski, R. & Szczurek, M. (2000). Enhanced X-ray emission in the 1-keV range from a laser-irradiated gas puff target produced using the double-nozzle setup. *Appl. Phys. B: Lasers Opt.* **70**, 305–308.

Fritzsche, S., Grum-Grzhimailo, A.N., Gryzlova, E.V. & Kabachnik, N.M. (2011). Sequential two-photon double ionization of the 4d shell in xenon. *J. Phys. B: At. Mol. Opt. Phys.* **44**, 175602.

Harilal, S.S. (2004). Spatial and temporal evolution of argon sparks. *Appl. Opt.* **43**, 3931–3937.

Hong, Y.C., Uhm, H.S., Chun, B.J., Lee, S.K., Hwang, S.K. & Kim, D. Su. (2006). Microwave plasma torch abatement of NF_3 and SF_6. *Phys. Plasmas* **13**, 033508.

Huebner, W.F., Keady, J.J. & Lyon, S.P. (1992). Solar photo rates for planetary atmospheres and atmospheric pollutants. *Astrophys. Space Sci.* **195**, 1–294.

Imanaka, H. & Smith, M.A. (2009). EUV photochemical production of unsaturated hydrocarbons: Implications to EUV photochemistry in Titan and Jovian planets. *J. Phys. Chem. A* **113**, 11187–11194.

Kołos, R. (1995). A novel source of transient species for matrix isolation studies. *Chem. Phys. Lett.* **247**, 289–292.

Korotkov, R.Y., Goff, T. & Ricou, P. (2007). Fluorination of polymethylmethacrylate with SF_6 and hexafluoropropylene using dielectric barrier discharge system at atmospheric pressure. *Surf. Coat. Technol.* **201**, 7207–7215.

Lallement, L., Gosse, C., Cardinaud, C., Peignon-Fernandez, M.C. & Rhallabi, A. (2010). Etching studies of silica glasses in SF_6/Ar inductively coupled plasmas: Implications for microfluidic devices fabrication. *J. Vacuum Sci. Technol. A* **28**, 277.

Liptak, R.W., Devetter, B., Thomas, J.H., Kortshagen, U. & Campbell, S.A. (2009). SF_6 plasma etching of silicon nanocrystals. *Nanotechnology* **20**, 035603.

Matzen, M.K., Sweeney, M.A., Adams, R.G., Asay, J.R., Bailey, J.E., Bennett, G.R., Bliss, D.E., Bloomquist, D.D., Brunner, T.A., Campbell, R.B., Chandler, G.A., Coverdale, C.A., Cuneo, M.E., Davis, J.P., Deeney, C., Desjarlais, M.P., Donovan, G.L., Garasi, C.J., Haill, T.A., Hall, C.A., Hanson, D.L., Hurst, M.J., Jones, B., Knudson, M.D., Leeper, R.J., Lemke, R.W., Mazarakis, M.G., McDaniel, D.H., Mehlhorn, T.A., Nash, T.J., Olson, C.L., Porter, J.L., Rambo, P.K., Rosenthal, S.E., Rochau, G.A., Ruggles, L.E., Ruiz, C.L., Sanford, T.W.L., Seamen, J.F., Sinars, D.B., Slutz, S.A., Smith, I.C., Struve, K.W., Stygar, W.A., Vesey, R.A., Weinbrecht, E.A., Wenger, D.F. & Yu, E.P. (2005). Pulsed-power-driven high energy density physics and inertial confinement fusion research. *Phys. Plasmas* **12**, 055503.

Ogura, K., Yamada, H., Sato, Y. & Okamoto, Y. (1997). excitation temperature in high-power nitrogen microwave-induced plasma at atmospheric pressure. *Appl. Spectrosc.* **51**, 1496–1499.

Pavlov, A.V. (2014). Photochemistry of ions at d-region altitudes of the ionosphere: A review. *Surv. Geophys.* **35**, 259–334.

Peignon, M.C., Cardinaud, Ch. & Turban, G. (1991). Etching processes of tungsten in SF_6–O_2 radio-frequency plasmas. *J. Appl. Phys.* **70**, 3314.

Peterson, W.K., Brain, D.A., Mitchell, D.L., Bailey, S.M. & Chamberlin, P.C. (2013). Correlations between variations in solar EUV and soft X-ray irradiance and photoelectron energy spectra observed on Mars and Earth. *J. Geophys. Res. A* **118**, 7338–7347.

Peterson, W.K., Woods, T.N., Fontenla, J.M., Richards, P.G., Chamberlin, P.C., Solomon, S.C., Tobiska, W.K. & Warren, H.P. (2012). Solar EUV and XUV energy input to thermosphere on solar rotation time scales derived from photoelectron observations. *J. Geophys. Res.: Space Phys.* **117**, A05320.

Pilling, S., Andrade, D.P.P., do Nascimento, E.M., Marinho, R.R.T., Boechat-Roberty, H.M., de Coutinho, L.H., de Souza, G.G.B., de Castilho, R.B., Cavasso-Filho, R.L., Lago, A.F. & de Brito, A.N. (2011). Photostability of gas- and solid-phase biomolecules within dense molecular clouds due to soft X-rays Mon. *Not. R. Astron. Soc.* **411**, 2214–2222.

Plank, N.O.V., Blauw, M.A., van der Drift, E.W.J.M. & Cheung, R. (2003). The etching of silicon carbide in inductively coupled SF_6/O_2 plasma. *J. Phys. D* **36**, 482–487.

Saloman, E.B. (2004). Energy levels and observed spectral lines of xenon, XeI through XeLIV. *J. Phys. Chem. Ref. Data* **33**, 765–921.

Shim, K-H., Kil, Y-H., Yang, H.D., Park, B.K., Yang, J-H., Kang, S., Jeong, T.S. & Kimor, T.S. (2012). Characteristics of germanium dry etching using inductively coupled SF_6 plasma. *Mater. Sci. Semicond. Process.* **15**, 364–370.